Acta Neurochirurgica (2019) 161:247–256
https://doi.org/10.1007/s00701-018-3730-6

ORIGINAL ARTICLE - VASCULAR NEUROSURGERY - ANEURYSM

Magnitude and direction of aqueductal cerebrospinal fluid flow: large variations in patients with intracranial aneurysms with or without a previous subarachnoid hemorrhage

Erika Kristina Lindstrøm[1] · Geir Ringstad[2,3] · Angelika Sorteberg[3,4] · Wilhelm Sorteberg[4] · Kent-Andre Mardal[1,5] · Per Kristian Eide[3,4]

Received: 20 June 2018 / Accepted: 6 November 2018 / Published online: 15 November 2018

Abstract

Background Net cerebrospinal fluid (CSF) flow within the cerebral aqueduct is usually considered to be antegrade, i.e., from the third to the fourth ventricle with volumes ranging between 500 and 600 ml over 24 h. Knowledge of individual CSF flow dynamics, however, is hitherto scarcely investigated. In order to explore individual CSF flow rate and direction, we assessed net aqueductal CSF flow in individuals with intracranial aneurysms with or without a previous subarachnoid hemorrhage (SAH).

Methods A prospective observational study was performed utilizing phase-contrast magnetic resonance imaging (PC-MRI) to determine the magnitude and direction of aqueductal CSF flow with an in-depth, pixel-by-pixel approach. Estimation of net flow was used to calculate CSF flow volumes over 24 h. PC-MRI provides positive values when flow is retrograde.

Results The study included eight patients with intracranial aneurysms. Four were examined within days after their SAH; three were studied in the chronic stage after SAH while one patient had an unruptured intracranial aneurysm. There was a vast variation in magnitude and direction of aqueductal CSF flow between individuals. Net aqueductal CSF flow was retrograde, i.e., directed towards the third ventricle in 5/8 individuals. For the entire patient cohort, the estimated net aqueductal CSF volumetric flow rate (independent of direction) was median 898 ml/24 h (ranges 69 ml/24 h to 12.9 l/24 h). One of the two individuals who had a very high estimated net aqueductal CSF volumetric flow rate, 8.7 l/24 h retrograde, later needed a permanent CSF shunt.

Conclusions The magnitude and direction of net aqueductal CSF flow vary extensively in patients with intracranial aneurysms. Following SAH, PC-MRI may offer the possibility to perform individualized assessments of the CSF circulation.

Keywords Phase-contrast magnetic resonance imaging · Subarachnoid hemorrhage · Cerebral aqueduct · Cerebrospinal fluid flow

Erika Kristina Lindstrøm and Geir Ringstad contributed equally to this work.

This article is part of the Topical Collection on *Vascular Neurosurgery – Aneurysm*

Electronic supplementary material The online version of this article (https://doi.org/10.1007/s00701-018-3730-6) contains supplementary material, which is available to authorized users.

✉ Per Kristian Eide
peide@ous-hf.no; p.k.eide@medisin.uio.no

[1] Department of Mathematics, Faculty of Mathematics and Natural Sciences, University of Oslo, Oslo, Norway

[2] Department of Radiology and Nuclear Medicine, Oslo University Hospital, Rikshospitalet, Oslo, Norway

[3] Institute of Clinical Medicine, Faculty of Medicine, University of Oslo, Oslo, Norway

[4] Department of Neurosurgery, Oslo University Hospital, Rikshospitalet, Pb 4950 Nydalen, N-0424 Oslo, Norway

[5] Department of Numerical Analysis and Scientific Computing, Simula Research Laboratory, Fornebu, Norway

Abbreviations

ACOM	Anterior communicating artery
CSF	Cerebrospinal fluid
EVT	Endovascular treatment
ICA	Internal carotid artery
iNPH	Idiopathic normal pressure hydrocephalus
PC-MRI	Phase-contrast magnetic resonance imaging
ROI	Region of interest
SAH	Subarachnoid hemorrhage
SNR	Signal-to-noise ratio

Introduction

Aneurysmal subarachnoid hemorrhage (SAH) carries high morbidity and mortality rates [18]. One important consequence of the bleed is cerebrospinal fluid (CSF) circulation failure in both the acute and the chronic phases of the hemorrhage [3]. Particularly, patients presenting in severe clinical condition are prone to disturbances in the CSF circulation and development of secondary hydrocephalus [17]. A significant portion of individuals hence need temporary or permanent CSF diversion (shunt surgery) [3]. Blood in the subarachnoid space may affect CSF circulation in different ways; possible mechanisms include impaired CSF absorption along CSF efflux routes, including impaired glymphatic function, i.e., impaired paravascular transport of water and solutes [4, 5], and compensatory increase in ventricular CSF production [8].

In vivo assessment of CSF production has been performed with phase-contrast magnetic resonance imaging (PC-MRI) of aqueductal CSF flow in healthy individuals [6] and individuals with CSF circulation failure [14]. The same technology should be applicable in individuals with an intracranial aneurysm with or without SAH. Knowledge of individual CSF flow dynamics may then be helpful in selecting those that would gain the most of CSF diversion and shunt surgery [14].

To this end, we performed a prospective, observational study of PC-MRI in individuals with intracranial aneurysms in order to explore CSF production rates and direction based on assessments of net aqueductal CSF flow. The hypothesis was that net CSF flow within the cerebral aqueduct is antegrade, i.e., from the third to the fourth ventricle and in the range of 500–600 ml over 24 h, which corresponds to established knowledge [7].

Materials and methods

Patients

The study included patients with ruptured and unruptured intracranial aneurysms that were managed at the Department of Neurosurgery, Oslo University Hospital-Rikshospitalet, Oslo, Norway, during the years 2015–2016.

The study was approved by the Institutional data protection and privacy council (Approval 2014/8139) and The Regional Committee for Medical and Health Research Ethics (REK), Region South-East, Norway (Approval 2014/633). Patients were included after oral and written informed consent.

The patients underwent standard clinical management. When MRI was indicated for clinical reasons, PC-MRI sequences were added as part of the study protocol. Consecutive patients who were willing to participate were included in the study, regardless of the underlying diagnosis.

Phase-contrast MRI

The PC-MRI information was acquired from different Siemens scanners (Siemens Healthcare, Erlangen, Germany) (1.5-T Aera, 1.5-T Avanto, and 3-T Skyra) equipped with standard head coils (range 12–20 channels) and an acquisition plane perpendicular to the aqueduct at mid aqueductal level. Scanning parameters were typically as follows: repetition time (TR) = 23 ms/echo time (TE) = 7 ms, voxel size 0.63 × 0.63 × 5.00 mm^3, matrix of 256 × 256 pixels, field of view (FOV) 16 cm, and 30–40 phases with retrospective peripheral cardiac gating. Velocity encoding (V_{enc}) was set after performing "V_{enc} scouts" to identify the value which rendered for optimal sensitivity for flow velocity assessment and at the same time avoid flow aliasing. V_{enc} values thus ranged from 8 to 25 cm/s. The time length of the PC-MRI sequences was approximately 6 min, which is an ordinary time for PC-MRI acquisitions.

Image analysis

Regions of interest

The region of interest (ROI) defining the outer perimeter of the cerebral aqueduct (Fig. 1a) was manually defined from PC-MRI magnitude images using MATLAB® (R2014b, The MathWorks Inc., Natick, MA, USA) and were performed by a neuroradiologist (GR) with technical assistance by a mathematician (EKL). Thereafter, the velocities from each of the chosen pixels were carefully evaluated by plotting the pixel velocities in MATLAB. Any included pixel that displayed unexpected behavior (flow signal unlikely to represent physiological CSF flow) was excluded from the ROI in further processing (a total of two pixels, one pixel in two patients) by the assumption it would represent an artifact, or noise, not flow signal. In addition, a reference ROI was defined close to the original region of interest (aqueduct), in order to quantify the noise level. One example of a ROI and reference ROI is visualized in Fig. 1b. One pixel that was included in the original ROI, but after velocity evaluation was excluded from the data set, is highlighted in yellow (Fig. 1b). Figure 1c

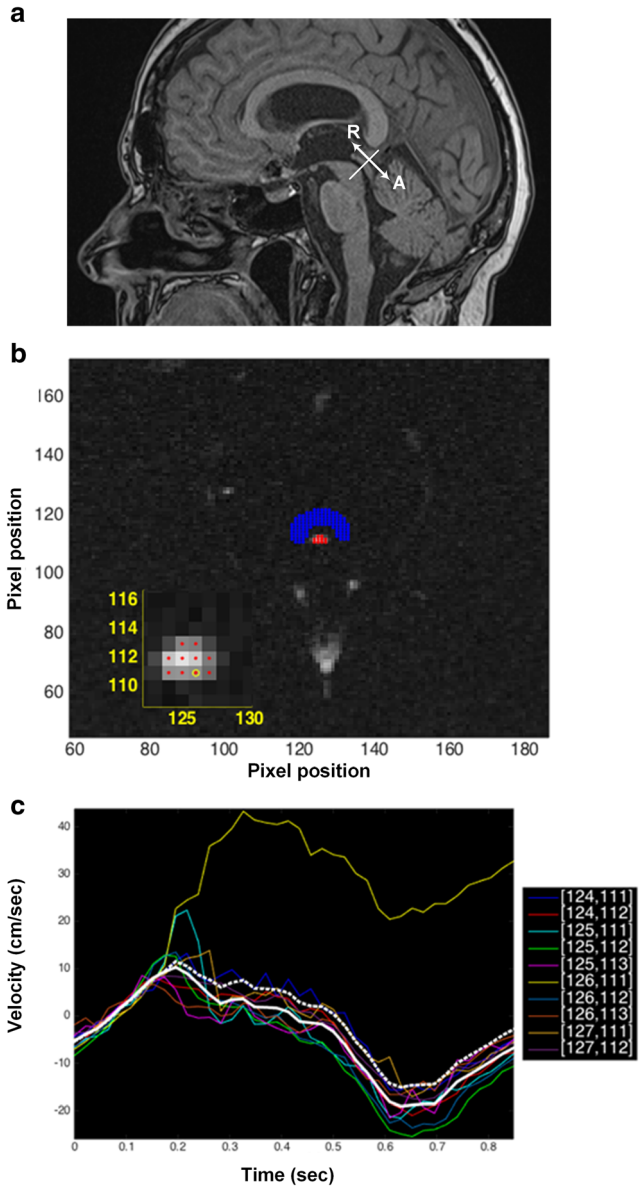

Fig. 1 **a** A sagittal T1-weighted MRI shows the Sylvian aqueduct of patient ID 8. During each cardiac cycle, the CSF pulsates in both the antegrade (A) and retrograde (R) directions. In this cohort, net CSF flow was retrograde in 5/8 and antegrade in 3/8 individuals. **b** The ROI within the Sylvian aqueduct is highlighted with red dots. Reference ROIs are highlighted with blue dots. A zoom of the regions of interest is shown in the left corner where pixel (126,111) is highlighted in yellow. **c** The pixel velocities of the individual ROIs are shown. Pixel (126,111) displays an unphysical behavior and is excluded from the ROI. White dotted line shows the mean velocity of the original ROI, and white solid line shows mean velocity after pixel (126,111) has been excluded

visualizes the pixel velocities from the same patients, where the excluded pixel shows flow unlikely to be physiological and was thereafter excluded from the ROI. The mean velocity is largely affected by the excluded pixel. The number of pixels included differed somewhat between patients, as presented in Fig. 2.

Velocities and aliasing

Recorded velocities were converted by linear transformation from pixel values to centimeters per second by applying the velocity encoding using MATLAB® in accordance with previously reported analyses of CSF flow data in the craniocervical junction [15]. A filter was designed to correct pixels that contained aliased velocities, e.g., velocities that exceeded the V_{enc}. The filter was activated if the temporal velocity difference in one pixel was larger than 1.1 times the velocity encoding. In that case, the aliased pixel was replaced by $v = v_a \pm 2 \times V_{enc}$, where v is the filtered velocity, v_a is the aliased pixel value, and V_{enc} is the velocity encoding.

The recorded velocities in the reference ROI were converted to centimeters per second and thereafter averaged over the number of pixels to achieve a mean velocity of the noise (Fig. 1c; Fig. 3). The calculated mean velocity was considered bias in the data set (baseline flow velocity offset). The original velocity data were corrected for biasing by subtracting the noise mean velocity from each pixel velocity in the region of interest.

The noise level was estimated by calculating the signal-to-noise ratio (SNR) defined as

$$SNR = 10 \times \log\left(\frac{P_S}{P_N}\right)$$

where P_S is the power of the signal and P_N is the power of the noise (power is defined as the amplitude squared). We defined the signal as the mean velocity in the original region of interest and calculated SNR for each pixel in the reference ROI. To achieve one representative SNR for each data set, we averaged the calculated SNR numbers.

Figure 1b, c illustrates pixel and mean velocities in the ROI and reference ROI of the Sylvian aqueduct of patient 8.

Volumetric flow calculations

Volumetric flow rate Q (ml/s) in the ROI was calculated by computing the sum of each pixel velocity over one cycle multiplied with pixel size

$$Q(t) = \left(\sum_{i=1}^{n} v_i\right) \times dx \times dy$$

The positive and negative contributions of the volumetric flow rate, showing retrograde and antegrade aqueductal flow, respectively, were calculated separately in the same manner, but instead of summing all pixels in the ROI, the positive and negative velocities were extracted before the calculation. The advantage of pixel-by-pixel calculations is that this method captures the contributions also in case of synchronous bidirectional flow. Figure 4a–h shows bidirectional flow within the cerebral aqueduct. The 2D and 3D visualizations show

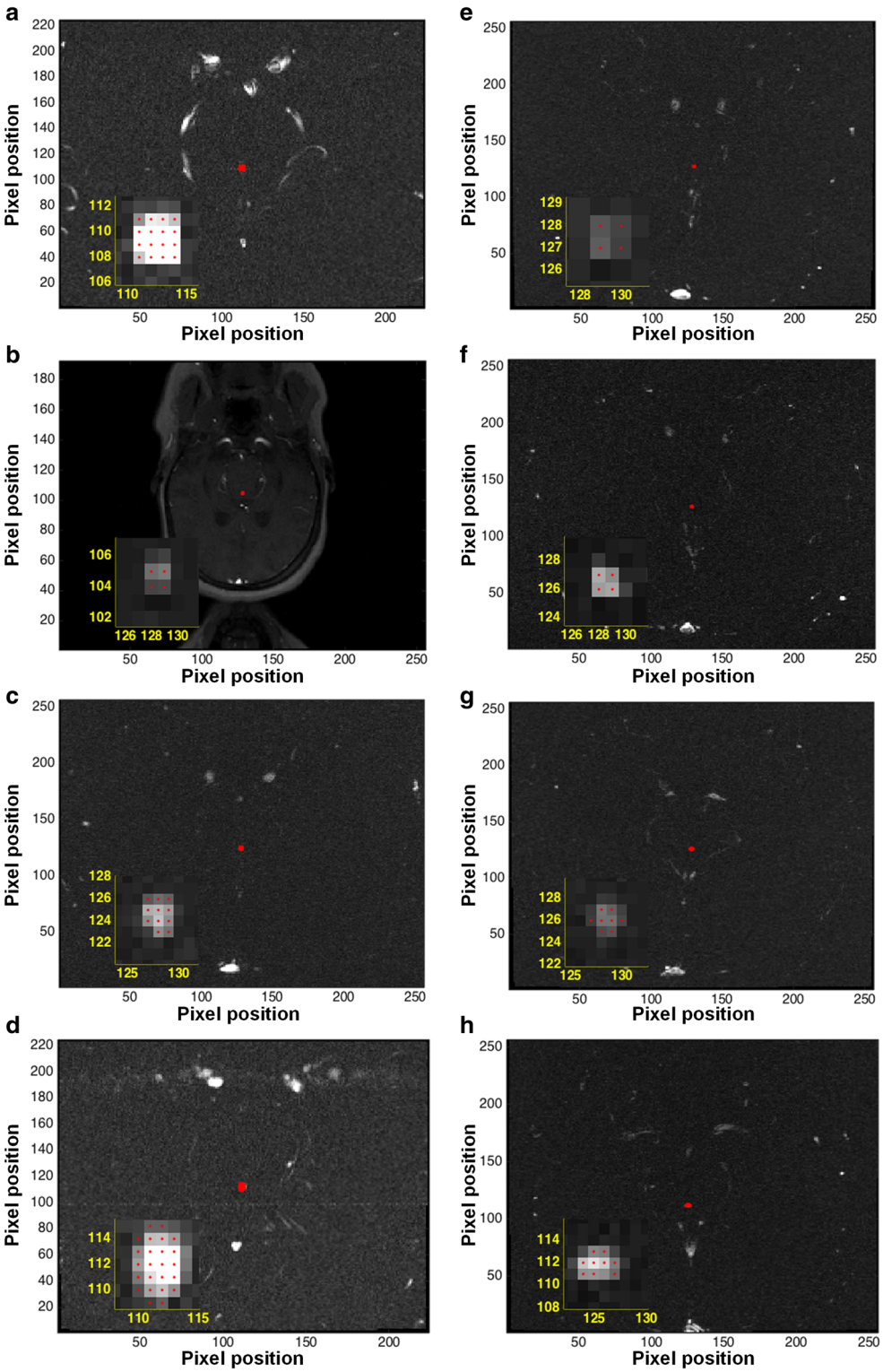

Fig. 2 The regions of interest (shown in red) within the Sylvian aqueduct with included pixels are shown for patients 1 (**a**), 2 (**b**), 3 (**c**), 4 (**d**), 5 (**e**), 6 (**f**), 7 (**g**), and 8 (**h**). As shown, the number of pixels ranged between 4 and 24

information that may get lost if the velocities over the ROI are averaged before calculating the volumetric flow rate.

The net volume over one cardiac cycle was calculated by discrete integration (trapezoidal method) of Q over time:

$$\text{Net volume} = \frac{dt}{2} \sum_{i=1}^{n} \left(Q(t_{i+1}) + Q(t_i) \right)$$

Volumes over one cycle in cranial and caudal direction were calculated by integration of positive and negative

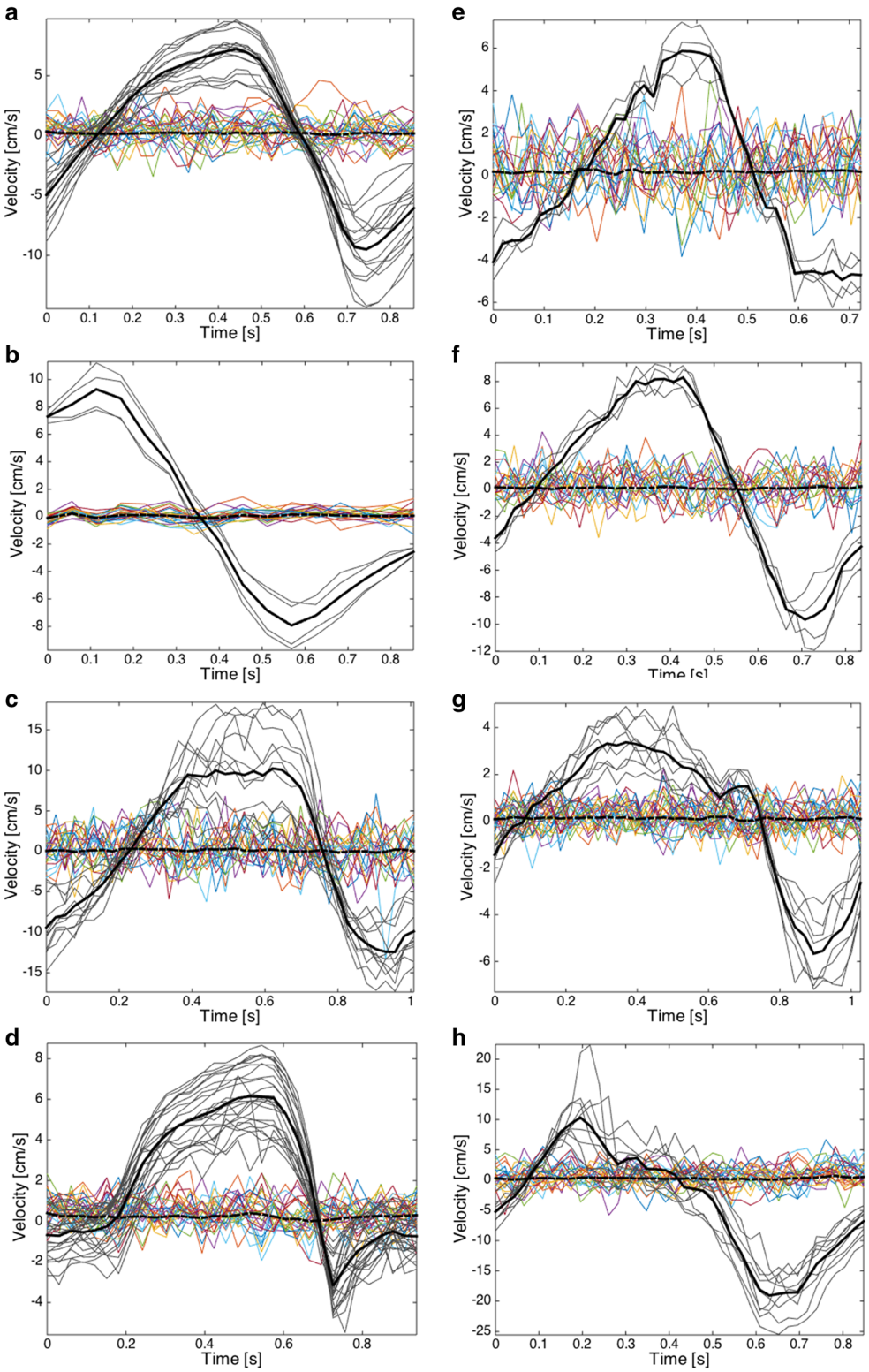

Fig. 3 CSF flow velocity for the different pixels, mean flow velocity of all pixels (dark line), noise level of reference tissue, and mean noise level (dark stippled line) are shown for patients 1 (**a**), 2 (**b**), 3 (**c**), 4 (**d**), 5 (**e**), 6 (**f**), 7 (**g**), and 8 (**h**)

volume fluxes over time. The total volume during one cycle was determined by the sum of the positive volume and the absolute value of the negative volume. Positive volume values are directed cranial in relation to the aqueduct and negative volume values are directed caudal, respectively.

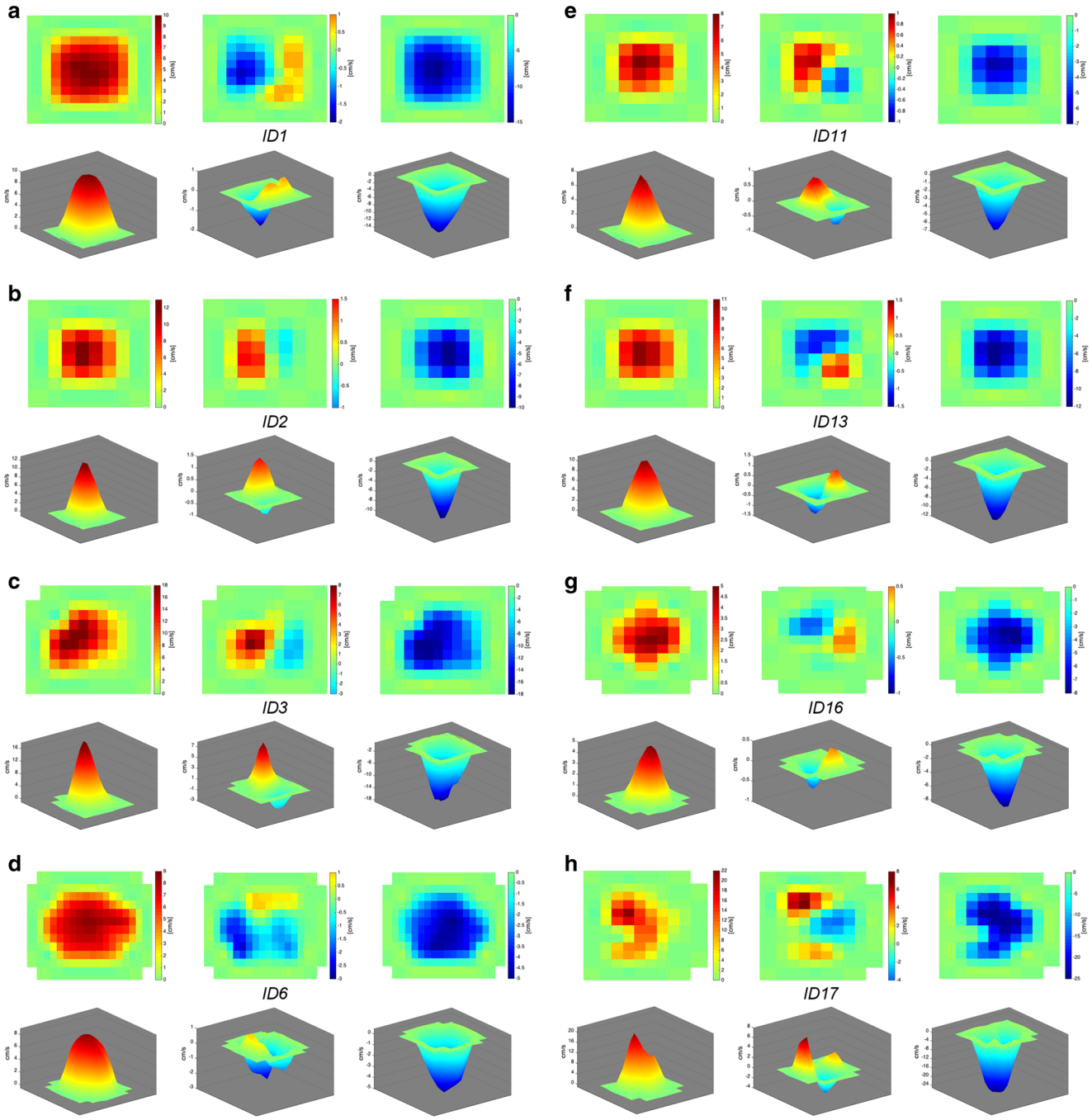

Fig. 4 The 2D and 3D visualizations of aqueductal CSF flow are presented for patients 1 (**a**), 2 (**b**), 3 (**c**), 4 (**d**), 5 (**e**), 6 (**f**), 7 (**g**), and 8 (**h**). The maximum velocity for each pixel is shown. For 3D visualizations, the pixel resolution is defined by a factor 2. Instead of 256 × 256 pixels, we get 512 × 512 pixels, which does not change the velocities, only pixel size. In addition for visualizing purposes, the data is interpolated to get a smoother transition between the pixels

Results

Patients

During the time period October 2015–May 2016, 14 patients with intracranial aneurysms underwent PC-MRI. Due to motion artifacts or weak PC-MRI flow signal, the cerebral aqueduct could not be reliably defined in six of them, leaving a patient cohort of eight for analysis. Table 1 provides demographic and management data of the eight patients. Four of them were investigated within days after their bleed; three were studied in the chronic stage after SAH while one patient had an unruptured intracranial aneurysm. Among the four patients investigated shortly after their bleed, patient ID 6

Table 1 Demographic and treatment information about included individuals

PatID	Age	Gender	Type of aneurysm repair and aneurysm localization	Time from SAH	Symptoms at time of investigation	Temporary CSF drain after SAH	Need of permanent shunt	Evan's index
1	58	F	EVT, ACOM aneurysm	11 months	Headache, fatigue, dizziness, memory deficits	No	No	0.29
2	46	F	EVT, ICA aneurysm	10 days	Headache, nausea	No	No	0.29
3	49	M	EVT, ACOM aneurysm	2 days	Headache, nausea	No	No	0.28
4	71	F	EVT, ACOM aneurysm	13 days	Unconscious, artificial respiration	Yes	Yes	0.31
5	42	F	Clip, ACOM aneurysm	6 years	Headache, fatigue, dizziness	No	No	0.27
6	51	F	EVT, ACOM aneurysm	8 days	Headache, mobilized to chair	No	No	0.25
7	53	F	EVT, ICA aneurysm	Unruptured	Impaired vision left eye	–	No	0.31
8	68	F	EVT, ICA aneurysm	7 months	Fatigue	No	No	0.34

F, female; *M*, male; *EVT*, endovascular treatment; *ACOM*, anterior communicating artery; *ICA*, internal carotid artery

had received a lumbar drain for temporary CSF diversion prior to investigation. The lumbar drain was, however, kept closed during the time of MRI acquisition.

Phase-contrast MRI

Figure 2 shows the ROIs within the cerebral aqueduct for each of the eight patients. The numbers of pixels as well as the areas of ROIs are shown in Table 2. Median 9 pixels (ranges 4–24 pixels) were included incorporating median 0.037 cm^2 (ranges 0.016–0.063 cm^2); the SNR was median 13.8 (ranges 9.2–22.6). Figure 3 presents the CSF flow velocities for each pixel of the individual patients, also showing values for reference ROIs. 2D and 3D presentations of CSF flow velocity within the ROIs are presented in Fig. 4.

Net aqueductal CSF flow was antegrade (out of third ventricle) in 3/8 and retrograde (towards third ventricle) in 5/8 patients (Table 2). For all patients combined, the absolute net aqueductal CSF volumetric flow rate per cardiac cycle was median 0.01 ml (ranges 0.001–0.126 ml) and the estimated net aqueductal CSF flow volume/24 h was median 898 ml (ranges 69 ml to 12.87 l). The CSF volumetric flow rate and direction of the net flow for individual patients are further illustrated in Fig. 5. One patient (ID 4) later needed insertion of a permanent shunt from the supratentorial ventricle to the peritoneal cavity; this individual had an estimated net retrograde aqueductal CSF volumetric flow rate of 8.7 l/24 h (Table 2). The patient (ID 7) with an unruptured intracranial aneurysm had an estimated net retrograde aqueductal CSF volumetric flow rate of 288 ml/24 h.

Table 2 Phase-contrast MRI–derived CSF volumetric flow rate and direction at the cerebral aqueduct

PatID	ROI area (cm^2)	ROI number (pixels)	SNR (pixel-by-pixel)	dP (mmHg/cm)	Total volumetric flow rate (ml/cycle)	Net volumetric flow rate (ml/cycle)	Estimated net volumetric flow rate (l/24 h)	Direction of net flow
1	0.039	16	13.945	0.106	0.163	0.002	0.203	R
2	0.063	4	22.589	0.060	0.300	0.016	1.647	A
3	0.043	11	11.051	0.167	0.327	0.016	1.353	R
4	0.058	24	12.762	0.105	0.159	0.094	8.709	R
5	0.016	4	9.218	0.152	0.037	0.001	0.069	A
6	0.016	4	13.777	0.131	0.068	0.004	0.442	R
7	0.031	8	12.579	0.083	0.079	0.003	0.288	R
8	0.035	9	14.496	0.203	0.242	0.126	12.869	A
Median (ranges)	0.037 (0.016–0.063)	9 (4–24)	13.269 (9.218–22.589)	0.118 (0.060–0.203)	0.161 (0.037–0.327)	0.010 (0.001–0.126)	0.898 (0.069–12.869)	

Data presented as absolute values

ROI, region of interest; *SNR*, signal-noise-ratio; *dP*, pressure gradient cerebral aqueduct; *A*, antegrade; *R*, retrograde

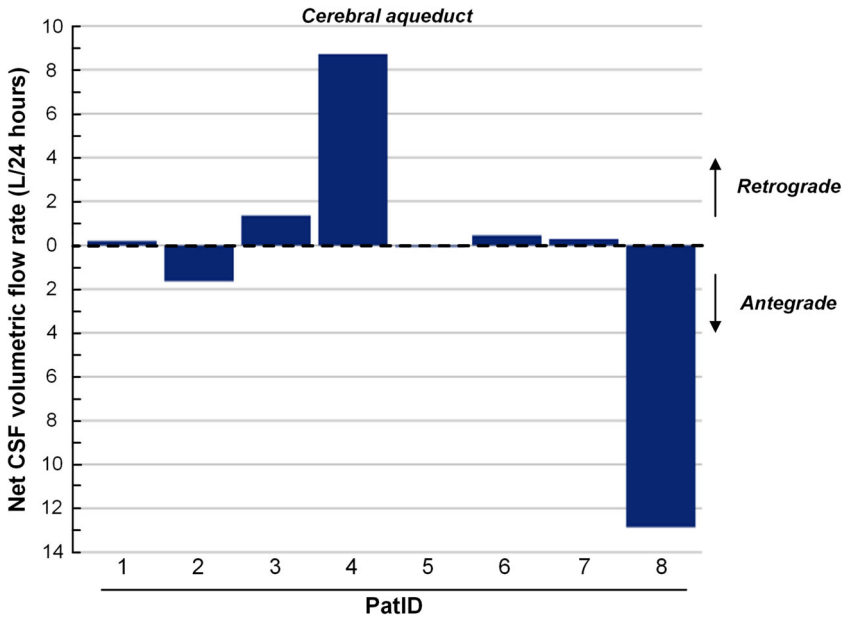

Fig. 5 The estimated net aqueductal CSF volumetric flow rate over 24 h is presented for each of the eight individual patients

Discussion

This observational study demonstrates that both the volumetric flow rate and direction of net aqueductal CSF flow may vary considerably between patients with intracranial aneurysms with or without a previous SAH. Our findings thus do not support the established knowledge that net aqueductal CSF flow in general is directed antegrade from the third to the fourth ventricle and with magnitude of about 500–600 ml/24 h.

Patients

Our patient cohort was both small and mixed. With regard to age, there were six middle-aged (42–58 years) and two elderly (68 and 71 years) patients. Four patients had ACOM aneurysms and the other three ICA aneurysms. With regard to aneurysm rupture, four patients were investigated within days after their bleed; three were studied in the chronic stage after SAH while one patient had never bled. The small sample size limits pooling of data in accordance with type of treatment (endovascular versus surgical treatment) and prediction of need of shunt treatment. Therefore, the present results are preliminary. To study CSF volumetric flow rates that may be generalized into a larger population, more patients with unruptured intracranial aneurysms and healthy subjects should be investigated.

Phase-contrast MRI

The applied methodology for PC-MRI post-processing represents the major strength of the work. Different from previous studies where CSF flow was estimated from PC-MRI acquisitions (reviewed by Ragunathan and Pipe [13]), we considered each pixel separately within the ROI defining the cerebral aqueduct. Flow aliasing had been avoided to a large extent by a pre PC-MRI "V_{enc} scout" scan and then corrected for post-scan by a specially designed filter at a single-pixel level. Unphysical flow patterns are detected and the corresponding pixel may be excluded from the ROI. These kinds of extreme velocities would otherwise affect the calculations. Positive and negative velocities in bidirectional flow will often cancel out each other when averaging velocities in the ROI to achieve a representative mean velocity; hence, averaging would reduce the calculated flow volumes. The methodology applied in this work captures the contribution from bidirectional flow. Furthermore, the signal within nearby reference tissue was assessed to correct for background noise (see Fig. 3) and to quantify the noise level. It was difficult to obtain reliable ROIs within the aqueduct in 6/14 individuals, providing a cohort of only 8 patients. The challenge with obtaining reliable ROIs represents a weakness of the PC-MRI methodology. On the other hand, due to a conservative approach to selection of technically successful PC-MRI exams, the present results could be considered based on robust observations and thus valid.

The present pixel-pixel-based analysis of PC-MRI acquisitions has previously been used in analysis of volumetric CSF flow rate in the cerebral aqueduct of 26 idiopathic normal pressure hydrocephalus (iNPH) patients [9]. We also validated the methodology in four healthy volunteers and performed five repeated MRI acquisitions in each healthy subject that showed good repeatability of the method [9]. Based on our experience with this method, we find it unlikely that the large net CSF volumes in two individuals were artefactual caused by erroneous analysis.

In this study, different MRI scanners were used, which might cause greater variation in SNRs. In the study from our group [9], however, the SNRs were larger even though the same MRI machine was used in all study subjects. We therefore believe MRI machine-related differences were minor in this present study.

Aqueductal CSF volumetric flow rate and CSF production

From our findings using PC-MRI during a 6-min time period, we estimated net aqueductal CSF flow rate over 24 h. The presently reported aqueductal CSF volumetric flow rates/24 h differ largely from previously reported CSF production rates. It is generally considered that the ventricular CSF production rate is about 0.35–0.40 ml/min, which corresponds to about 500–600 ml/24 h [1]. It should be noted, however, that previous, invasive methods for assessing daily CSF production rates, such as the Pappenheimer technique, have significant limitations [1, 11, 12], and the method would be seriously flawed by extra-ventricular CSF formation, which is suggested by our finding of net retrograde CSF flow at the aqueduct level.

While it has been considered that CSF production may vary somewhat, differences between disease categories have not been defined. Our patient ID 7 with an unruptured intracranial aneurysm had a net retrograde aqueductal CSF volumetric flow rate of 288 ml/24 h. In contrast, our two elderly patients (ID 4 and ID 8) had extreme estimated net aqueductal CSF volumetric flow rates (8.7 l/24 h and 12.9 l/24 h, respectively), one antegrade and the other retrograde. The finding of a reversed extreme net aqueductal CSF flow corroborates with previous observations in 21 elderly patients (median age 74 years, ranges 56–84 years) with idiopathic normal pressure hydrocephalus (iNPH), in whom net aqueductal flow, as assessed by PC-MRI, was retrograde in 16 and antegrade in 5 of them [14]. The estimated net aqueductal CSF volumetric flow rate was median 1.1 l/24 h (ranges 40 ml/24 h to 18.4 l/24 h) in the total cohort of 21 iNPH patients and median 1.2 l/24 h (ranges 40 ml/24 h to 18.4 l/24 h) in the 16 cases with net retrograde CSF flow [14]. We found comparable net CSF volumetric flow rates when using the presently described pixel-pixel approach [9]. Moreover, the finding of retrograde flow in iNPH corroborates with another study [16] reporting that intrathecal gadobutrol as CSF tracer distributed rapidly to the third and lateral ventricles, indicative of retrograde aqueductal CSF flow, a phenomenon distinctly different from non-hydrocephalic cases.

Pressure gradients are decisive for the direction of flow; this also applies for the direction of net CSF flow in the cerebral aqueduct (pressure gradient dP; see Table 2). Hence, retrograde flow of CSF from the fourth to the third ventricle is caused by a positive pressure gradient, i.e., lower pressure in the third than in the fourth ventricle. In 5/8 of the present patients, net CSF flow was retrograde, meaning that pressure was lower in their third than in their fourth ventricle at the time of data acquisition. Further studies are needed to determine why third ventricular pressure is lower in these patients. We remark that our calculated pressure gradient is obtained from the PC-MRI velocities and refer to the dynamic pressure gradient. The effect of gravity in terms of a static pressure gradient is ignored.

Regarding patient ID 8 with an extreme antegrade flow of CSF, it is tempting to speculate about possibly increased ventricular CSF production. In line with this reasoning, previous animal studies have provided evidence of upregulated CSF production from choroid plexus after SAH [8].

It should be noted that aqueductal CSF flow assessed from one PC-MRI acquisition may not be extrapolated to reliably predict the daily CSF production. While the presently described cardiac-gated PC-MRI refers to CSF flow during the cardiac cycle, recent evidence shows that respiration may extensively impact CSF flow in addition to the cardiac heart beats [2]. Respiratory effects may, however, be averaged out at PC-MRI [20]. The role of circadian rhythm also underlines the dynamics of CSF production. At nighttime, it has been reported a nearly fourfold increase in CSF production rate [10], and glymphatic CSF flow through brain tissue increases steeply during sleep [19]. The volume of CSF production provided here, from daytime scans, may hence be considered minimum values.

As each patient presently was investigated only over a short time period and only once, our study provides no information with regard to possible temporal changes in magnitude and direction of aqueductal CSF flow in individual patients. Indeed, in our calculations, we assume similar net aqueductal flow during a 24-h period. Given this is fairly correct, however, our findings indicate that the CSF production rate may be considerably larger than previously assumed. It also indicates that, at least in some individuals, a large amount of CSF could be produced by other means and in other places than the choroid plexus of the cerebral ventricles. To sum up, the study highlights a substantial variation in aqueductal CSF volumetric flow rate and direction between patients.

Future prospects

Assessment of aqueductal CSF flow using PC-MRI may become useful for determining the type of CSF circulation failure. Tentatively, it may be suggested that net aqueductal CSF volumetric flow rates above certain thresholds may indicate a need for CSF diversion surgery. Given the large variation of data, more individuals need to be assessed. Also, we need to further address how CSF flow may change with age. Based on the present results, we still cannot conclude how PC-MRI can

be used in the clinical management of patients with intracranial aneurysms.

In a previous study, idiopathic normal pressure hydrocephalus patients with signs of reduced intracranial compliance (by increased ICP pulsatility), and thus expected to be shunt responders, where characterized by net retrograde aqueductal CSF flow, which reversed after shunting [14]. This corroborates with our patient ID 4 with high, retrograde CSF flow rate that became shunt dependent. The current study design and sample size limited us from exploring the possible role of aqueductal net flow direction in the selection of patients to CSF diversion; however, further studies could possibly improve the selection of SAH patients in need of a permanent CSF shunt.

Conclusions

Magnitude of aqueductal CSF volumetric flow rate varies extensively in patients with intracranial aneurysms and indicates that CSF production volumes may potentially be much larger than previously acknowledged. Net retrograde CSF flow at the aqueduct level opens for significant contributions to CSF formation outside the ventricular system.

Funding Department of Neurosurgery, Oslo University Hospital, Rikshospitalet, Oslo, Norway

Compliance with ethical standards

Conflict of interest The authors declare that they have no conflict of interest.

Ethical approval All procedures performed in studies involving human participants were in accordance with the ethical standards of the institutional and/or national research committee and with the 1964 Helsinki Declaration and its later amendments or comparable ethical standards.

For this type of study, formal consent is not required.

Informed consent Informed consent was obtained from all individual participants for whom identifying information is included in this article.

References

1. Brinker T, Stopa E, Morrison J, Klinge P (2014) A new look at cerebrospinal fluid circulation. Fluids and barriers of the CNS 11:10
2. Dreha-Kulaczewski S, Joseph AA, Merboldt KD, Ludwig HC, Gartner J, Frahm J (2015) Inspiration is the major regulator of human CSF flow. J Neurosci 35:2485–2491
3. Erixon HO, Sorteberg A, Sorteberg W, Eide PK (2014) Predictors of shunt dependency after aneurysmal subarachnoid hemorrhage: results of a single-center clinical trial. Acta Neurochir 156:2059–2069
4. Gaberel T, Gakuba C, Goulay R, Martinez De Lizarrondo S, Hanouz JL, Emery E, Touze E, Vivien D, Gauberti M (2014) Impaired glymphatic perfusion after strokes revealed by contrast-enhanced MRI: a new target for fibrinolysis? Stroke 45:3092–3096
5. Goulay R, Flament J, Gauberti M, Naveau M, Pasquet N, Gakuba C, Emery E, Hantraye P, Vivien D, Aron-Badin R, Gaberel T (2017) Subarachnoid hemorrhage severely impairs brain parenchymal cerebrospinal fluid circulation in nonhuman primate. Stroke 48:2301–2305
6. Huang TY, Chung HW, Chen MY, Giiang LH, Chin SC, Lee CS, Chen CY, Liu YJ (2004) Supratentorial cerebrospinal fluid production rate in healthy adults: quantification with two-dimensional cine phase-contrast MR imaging with high temporal and spatial resolution. Radiology 233:603–608
7. Johanson CE, Duncan JA 3rd, Klinge PM, Brinker T, Stopa EG, Silverberg GD (2008) Multiplicity of cerebrospinal fluid functions: new challenges in health and disease. Cerebrospinal Fluid Res 5:10
8. Kanat A, Turkmenoglu O, Aydin MD, Yolas C, Aydin N, Gursan N, Tumkaya L, Demir R (2013) Toward changing of the pathophysiologic basis of acute hydrocephalus after subarachnoid hemorrhage: a preliminary experimental study. World neurosurgery 80:390–395
9. Lindstrøm EK, Ringstad G, Mardal K-A, Eide PK (2018) Cerebrospinal fluid volumetric net flow rate and direction in idiopathic normal pressure hydrocephalus. NeuroImage Clinical 20:731–741
10. Nilsson C, Stahlberg F, Thomsen C, Henriksen O, Herning M, Owman C (1992) Circadian variation in human cerebrospinal fluid production measured by magnetic resonance imaging. Am J Phys 262:R20–R24
11. Oreskovic D, Klarica M (2014) Measurement of cerebrospinal fluid formation and absorption by ventriculo-cisternal perfusion: what is really measured? Croat Med J 55:317–327
12. Oreskovic D, Rados M, Klarica M (2017) Role of choroid plexus in cerebrospinal fluid hydrodynamics. Neuroscience 354:69–87
13. Ragunathan S, Pipe JG (2017) Radiofrequency saturation induced bias in aqueductal cerebrospinal fluid flow quantification obtained using two-dimensional cine phase contrast magnetic resonance imaging. Magnetic resonance in medicine
14. Ringstad G, Emblem KE, Eide PK (2016) Phase-contrast magnetic resonance imaging reveals net retrograde aqueductal flow in idiopathic normal pressure hydrocephalus. J Neurosurg 124:1850–1857
15. Ringstad G, Lindstrom EK, Vatnehol SAS, Mardal KA, Emblem KE, Eide PK (2017) Non-invasive assessment of pulsatile intracranial pressure with phase-contrast magnetic resonance imaging. PLoS One 12:e0188896
16. Ringstad G, Vatnehol SAS, Eide PK (2017) Glymphatic MRI in idiopathic normal pressure hydrocephalus. Brain 140:2691–2705
17. Sorteberg W, Slettebo H, Eide PK, Stubhaug A, Sorteberg A (2008) Surgical treatment of aneurysmal subarachnoid haemorrhage in the presence of 24-h endovascular availability: management and results. Br J Neurosurg 22:53–62
18. Suarez JI, Tarr RW, Selman WR (2006) Aneurysmal subarachnoid hemorrhage. N Engl J Med 354:387–396
19. Xie L, Kang H, Xu Q, Chen MJ, Liao Y, Thiyagarajan M, O'Donnell J, Christensen DJ, Nicholson C, Iliff JJ, Takano T, Deane R, Nedergaard M (2013) Sleep drives metabolite clearance from the adult brain. Science 342:373–377
20. Yildiz S, Thyagaraj S, Jin N, Zhong X, Heidari Pahlavian S, Martin BA, Loth F, Oshinski J, Sabra KG (2017) Quantifying the influence of respiration and cardiac pulsations on cerebrospinal fluid dynamics using real-time phase-contrast MRI. J Magn Reson Imaging 46:431–439